CrossMark

ORIGINAL PAPER

Effects of Annealing Temperature on Microstructure and Magnetic Properties of $Ni_{0.05}Zn_{0.95}Fe_2O_4$ Nanoparticles

L. Arda[1] · N. Dogan[2] · C. Boyraz[3]

Abstract The magnetic behavior of $Ni_{0.05}Zn_{0.95}Fe_2O_4$ nanoparticles synthesized by the sol–gel technique route was clarified To figure out the influence of annealing temperature on the structure of $Ni_{0.05}Zn_{0.95}Fe_2O_4$ particles, x-ray diffraction (XRD) tool was used and revealed spinel cubic structure without any secondary phases. The particle formation and sizes were obtained using scanning electron microscope (SEM). Elemental composition of the nanoparticles was also provided by an energy-dispersive x-ray analysis tool (EDX). The magnetic behaviors of the synthesized powders annealed at varying temperatures were determined by vibrating sample quantum design PPMS measurement system tool. The $M–H$ curves of the samples showed that the samples had S-shape but they reached no saturation state at the presence even at 30 kOe.

Keywords NiZn ferrites · Sol–gel · Nanoparticles · Magnetic measurement

✉ L. Arda
lutfi.arda@eng.bau.edu.tr

[1] Faculty of Engineering and Naturel Sciences, Department of Mechatronic Engineering, Bahcesehir University, Besiktas, Istanbul, 34349 Turkey

[2] Faculty of Science, Department of Physics, Gebze Technical University, Gebze, Kocaeli 41400, Turkey

[3] Faculty of Technology, Department of Mechanical Engineering, Marmara University, Goztepe, Istanbul, 34722 Turkey

1 Introduction

Ferrites are revealed as important magnetic materials due to their very appropriate dielectric loss, low eddy current losses, and high electrical resistivity. Therefore, they find a special place in technological applications over a wide range of frequencies [1]. A large class of compounds in ferrites has spinel structure. The well-known spinel unit cell has a close-packed cubic array of 32 oxygen anions, 8 Fe^{+2} ions, and 16 Fe^{+3} ions. A total of 24 metal cations are distributed among 8 tetrahedral interstice parts and 16 octahedral interstice parts [2, 3].

The scientific properties of spinel ferrite nanoparticle families bring a new point of view to the researchers and manufacturers with their magnetic and electronic properties and technological applications, respectively [4–9]. The importance of ferrites comes from vast technological applications, from radio frequencies to microwaves. In a wide range, ferrites present a number of special properties such as low losses for microwave applications and a relatively high resistivity at the carrier frequency [10, 11]. Varying synthesizing methods were tried to prepare ferrite nanoparticles such as mechanical milling [12], hydrothermal method [13–16], microwave route [17–20], sol–gel method [21], and surfactant-assisted route [22, 23].

The goal of this presented research is to determine the effects of annealing temperature on magnetic and structural properties of the Ni-doped Zn ferrites ($Ni_{0.05}Zn_{0.95}Fe_2O_4$) obtained by sol–gel method.

2 Experimental

To obtain the nanoparticle form of $Ni_{0.05}Zn_{0.95}Fe_2O_4$ compounds, Zn, Ni, and Fe-based alkoxide chemicals were

used. In synthesizing process, the chemicals, nickel 2,4-pentanedionate (Alfa Aesar), zinc acetylacetonate hydrate (Fluka), and iron 2,4-pentanedionate (Alfa Aesar) precursor materials were weighted in appropriate amounts and put into Pyrex container. The chemicals were then dissolved into methanol, acetylacetone, and glacial acetic acid mixture and mixed with a magnetic stirrer for 12 h to obtain homogeneous, clear, and stable solutions.

At room temperature, the beaker covers were taken out to remove the solvent using magnetic stirrer rotation. To evaporate the residual organics, the samples were preheated in a box furnace at a temperature range between 300 and 400 °C for 10 min. The samples were then grounded in an agate mortar and post-annealed in a box furnace at various temperatures (600–90 °C) under air to obtain a better atomic packing.

The crystal structure and particle size of powders were determined by x-ray diffraction pattern and Debye–Scherrer formula. Bruker D8 advance diffractometer model XRD with CuKα radiation was used for 2θ scans between 20° and 80° with 0.02° step and 0.5-s integration time. Scanning electron microscopy (SEM) measurements were performed at 15 kV to figure out the size and morphology of the magnetic nanoparticles (MNPs). To clarify the magnetic properties of MNPs, a quantum design vibrating sample magnetometer (QD-VSM) was used. Zero field cooling (ZFC) and field cooling (FC) measurements at 50 Oe were performed from 10 to 300 K. With the help of those measurements, blocking temperatures were revealed. Hysteresis curves (M–H) were separately performed between $+15$ and $−15$ kOe magnetic file for fixed 10, 50, 100, 200, and 300 K temperatures and thus the M–H curve components, coercivity field (H_c), remanent magnetization (M_r), and saturation magnetization (M_s) values were estimated.

3 Result and Discussion

XRD and SEM tools were used to analyze the crystal structure of the synthesized $Ni_{0.05}Zn_{0.95}Fe_2O_4$ magnetic particles. Effects of annealing temperature on the structures were investigated by XRD and results were exhibited in Fig. 1a. Using the MAUD program [24], the spinel cubic structure of space group Fd-3m without secondary phases (Fig. 1b) was obtained for $Ni_{0.05}Zn_{0.95}Fe_2O_4$ compositions by Rietveld analysis. The pattern peaks of the samples became sharper and narrower with increasing annealing temperature. Thus, we conclude that (a) lattice parameter directions of the synthesized nanoparticles were ordered by increasing annealing temperature. The most intense peak was defined as (311) from all other peaks and the full-width at half maximum (FWHM) of the ferrite particle XRD pattern was obtained
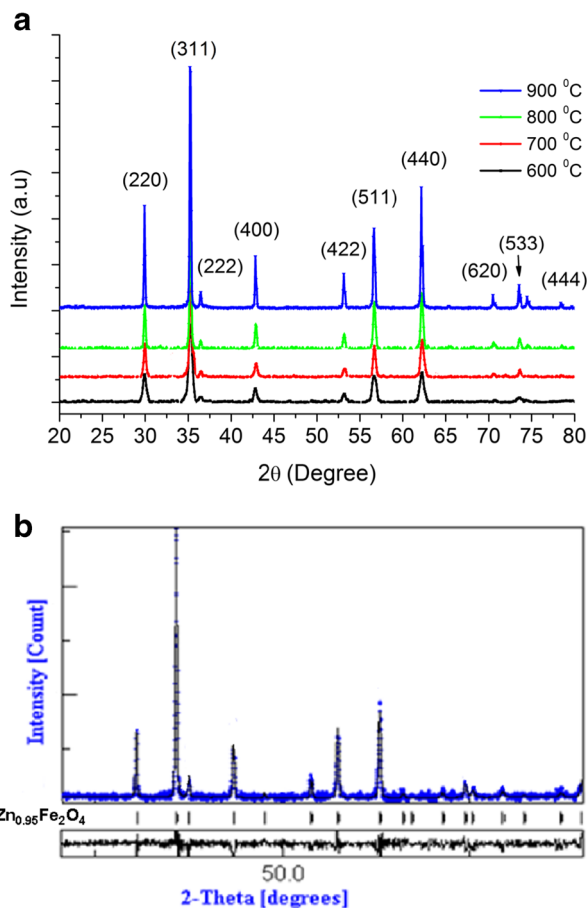

Fig. 1 a XRD powder patterns of $Ni_{0.05}Zn_{0.95}Fe_2O_4$ for different annealing temperature. **b** Rietveld analysis of $Ni_{0.05}Zn_{0.95}Fe_2O_4$ nanoparticles at 900 °C showing single phase

from (311) peak. The average particle size was calculated using the Debye–Scherrer equation.

$$D = 0.9\lambda / \beta \cos\theta \tag{1}$$

where λ, β, and θ_B are the x-ray wavelength of CuKα, the full width at half maximum (FWHM) of the diffraction peaks, and the angle of Bragg diffraction, respectively [20, 23, 25]. The average crystallite sizes of (3 1 1) peaks at different annealing temperatures were calculated by Scherrer's formula. The determined particle sizes from XRD analysis

Table 1 Temperature-dependent lattice parameter a and particle size variation

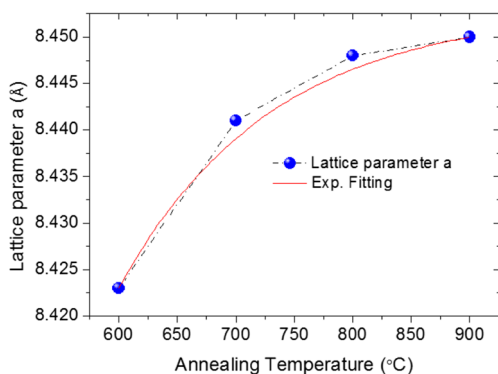| Annealing temperatures (°C)	Lattice parameter a (A)	Particle size (nm)
600	8.423	31.2
700	8.441	32.8
800	8.448	33.6
900	8.450	35.8

Fig. 2 Annealing temperature-dependent lattice parameter *a* variation

and Debye–Scherrer formula are given in Table 1 in which the values vary between 31 and 36 nm.

The Ni, ZnO, and Fe (NZFO) crystal size has been affected by increasing temperature, which is directly related to the crystallization. The crystallization phases of NZFO nanoparticles were directly affected by increasing annealing temperatures and at 400 °C low annealing temperature, Sheikh and Mathe have observed the diffraction peaks [26]. In our study, no impurity phase peaks were observed between wide temperature ranges (600–900 °C). Thus, the annealing temperature for NZFO particles should be well applied in commercial usage.

Annealing temperature-dependent lattice parameter *a* variation was provided by Fig. 2. We observed that the increment of annealing temperature of NZFO nano powders exhibited an exponential increase and saturation. A slight change of lattice parameter *a* variation was observed by after 800 and 900 °C by post-annealing temperature so the total behavior of the lattice parameter *a* variation was identified as exponential decreasing by red exponential fitting curve in Fig. 2.

Decreasing magnifies of SEM micro and nano images from 10 μm to 500 nm was monitored in Fig. 3a–c for the sample annealed at 900 °C temperature. When increasing the magnification from 10 μm to 500 nm frame, a cluster shape distribution was observed from Fig. 3. The elemental composition of NZFO nanoparticles annealed at 900 °C was obtained for K shell energies of all elements. According to the inset table presenting elemental composition results, the atomic percentage of NZFO nanoparticle was in a good harmony with desired stoichiometry of NZFO nanoparticles. The particle size of NZFO nanoparticles are approximately 100 nm because of agglomeration.
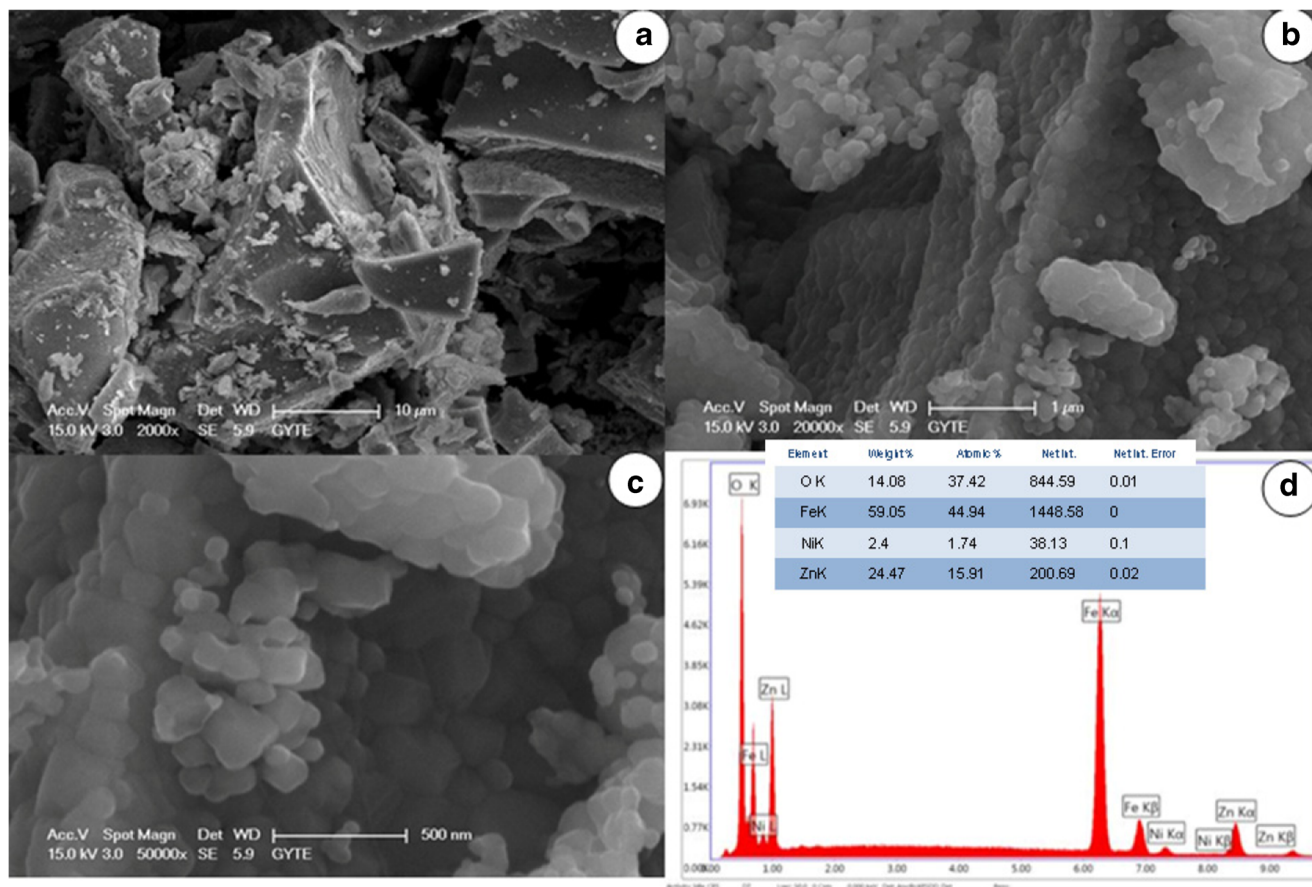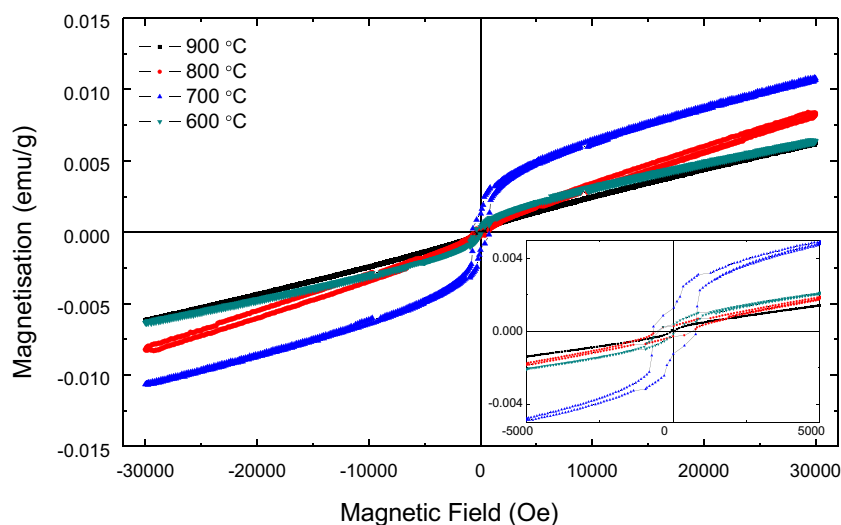

Element	Weight%	Atomic%	Net Int.	Net Int. Error
O K	14.08	37.42	844.59	0.01
FeK	59.05	44.94	1448.58	0
NiK	2.4	1.74	38.13	0.1
ZnK	24.47	15.91	200.69	0.02

Fig. 3 SEM micrograph and EDX spectrum of NZFO nanoparticles at 900 °C post-annealing temperature

Fig. 4 $M–H$ curves for NZFO nanoparticles with various annealing temperature at 300 K

Quantum design vibrating sample magnetometer (QDVSM) tool was used for the magnetic characterizations of $Ni_{0.05}Zn_{0.95}Fe_2O_4$ compositions. The magnetization of Ni–Zn ferrites as a function of the external field in the range of $\pm$ 30 kOe at 10 and 300 K was detailed for different annealing temperature. The $M–H$ curves have an S-shape but they cannot reach saturation state yet even with 30 kOe (Figs. 4 and 5).

The remanence magnetization values and the coercivity (H_c) values are directly taken from the M vs. H graph. Magnetic properties as remanent magnetization (M_r) and coercive field (H_c) are investigated with temperature is presented in Table 2. The M_r increases from 20×10^{-4} to 66×10^{-4} emu g^{-1} with the temperature at 10 K and for 300 K it varies from 8.15×10^{-5} to 3.6×10^{-4} emu g^{-1}

As can be seen from the inset graphs of Figs. 4 and 5, the magnetization value exhibits and increment with the external magnetic field strength at low field region However even

in the presence of a relatively high magnetic field at 30 kOe it does not reach a saturation state

Almost linear behavior is observed in the high field side of the curves with the external magnetic field so the measured saturation magnetization values vary with applied annealing temperature as well. The obtained saturation magnetization values from hysteresis loops of Fig. 6 are 11 $\times 10^{-3}$, 19 $\times 10^{-3}$ 31 $\times 10^{-3}$, 27 $\times 10^{-3}$, and 37 $\times 10^{-3}$ emu g^{-1} for the performed measurements in the order of decreasing tendency from 30 to 10 K respectively. This behavior is an indication of co-existing ferromagnetic and antiferromagnetic interactions. The unsaturated magnetization should point out mixed ferromagnetic interactions with the presence of strong antiferromagnetic inter-cluster interactions [27] Another reason should be attributed to non-saturated magnetization even at high fields as the existence of single small nanoparticles consisting of ferrimagnetically aligned core spins and a spin–glass-like surface layer have a

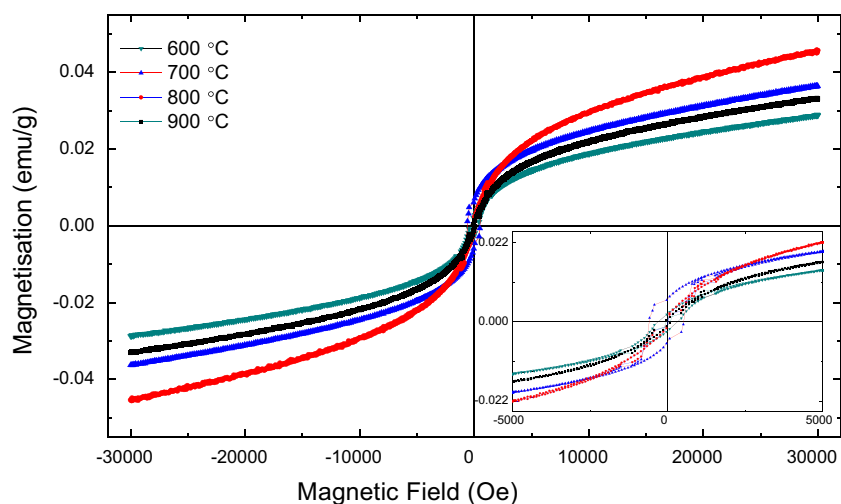**Fig. 5** $M–H$ curves for NZFO nanoparticles with various annealing temperature at 10 K

Table 2 The variation of magnetic parameters measured at 300 and 10 K for the samples annealed at wide temperature rates

Annealing temperature (°C)	Remanent magnetization $M_r (emug^{-1})$		Saturation Magnetization $M_s (emug^{-1})$		Coercivity Field $H_c (Oe)$	
	at 300 K	at 10 K	at 300 K	at 10 K	at 300 K	at 10 K
600	3.6×10^{-4}	23×10^{-4}	0.0064	0.028	301	330
700	1.26×10^{-4}	66×10^{-4}	0.011	0.037	35	410
800	3.2×10^{-5}	24×10^{-4}	0.0091	0.045	32	268
900	8.15×10^{-5}	20×10^{-4}	0.0063	0.033	75	336

core–shell morphology [27] In the absence of this layer, the magnetization of the particles would have saturated with the increases in the applied field.

The observed values of coercive field vary between 32–301 Oe at 300 K and 268–410 Oe at 10 K. Because of high coercivity, we can explain our sample as hard ferromagnetic. Changing of coercive field in our samples caused a difference in defect states and anisotropy contribution by the clusters of crystallites.

The magnetization-dependent temperature (M–T) was measured in Fig. 7 to reveal more details of the magnetic behaviors of the ZnO/Ni particles. Cooling of the samples under zero magnetic field (ZFC) make the total magnetizations of particles become nearly zero because of the randomly oriented magnetic moment of individual particles. It is found that the ZFC curve increases with decreasing temperature and exhibits a maximum (blocking temperature, T_B). Below T_B value, the curve starts to decrease. Blocking temperatures for the samples annealed at varying temperatures are 28.23 K (for 600 °C), 82 K (for 700 °C), 26 K (for 800 °C), and 28.4 K (for 900 °C). When nanoparticles are cooled to a very low temperature under a magnetic field, the magnetization direction of each particle is frozen in the direction of the field. There is a separation point for ZFC and FC curves, this point indicates a non-equilibrium magnetization below 168 K (for 600 °C), 213 K (for 700 °C), 190 K (for 800 °C), and 180 K (for 900 °C) for the ZFC case and additionally exhibits the irreversibility temperature, T_{irr}
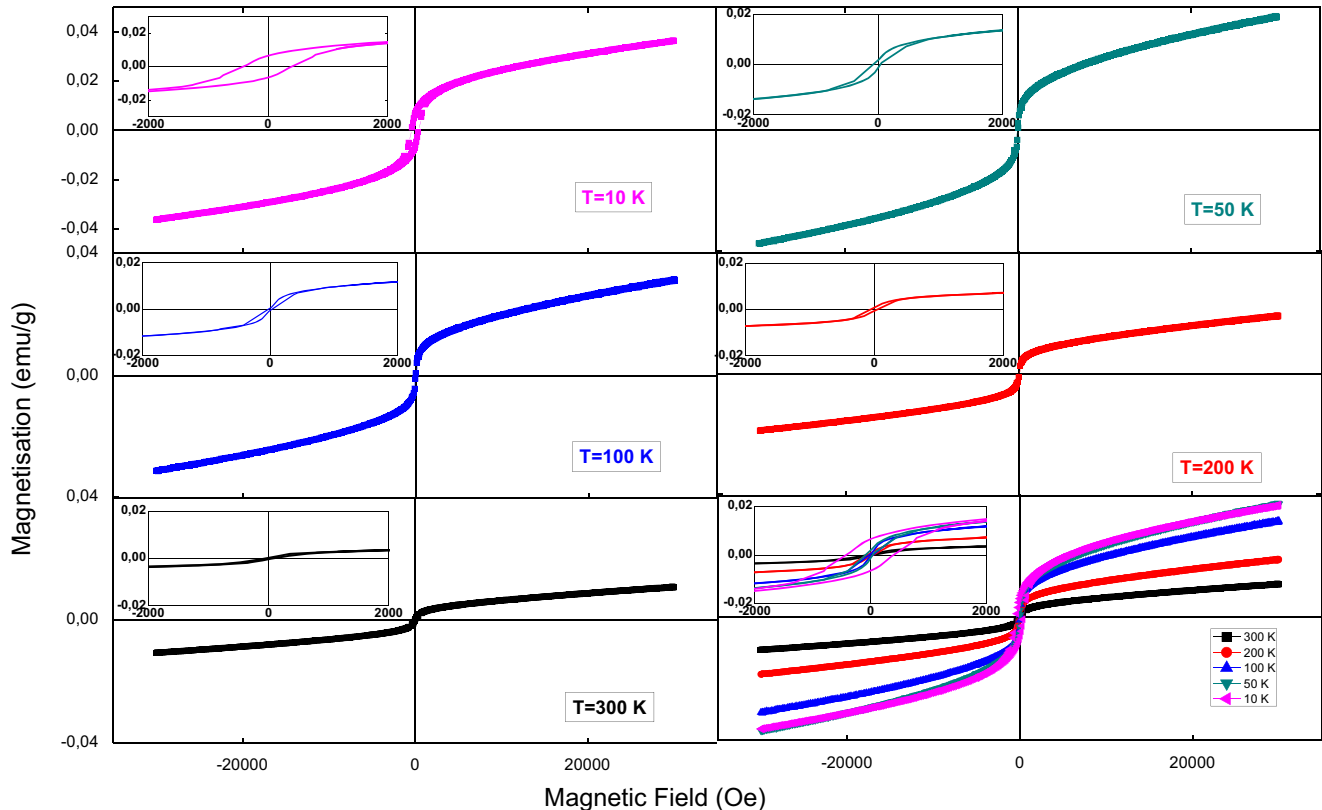

Fig. 6 M–H curves for NZFO particles for 700 °C annealing temperature at different temperatures
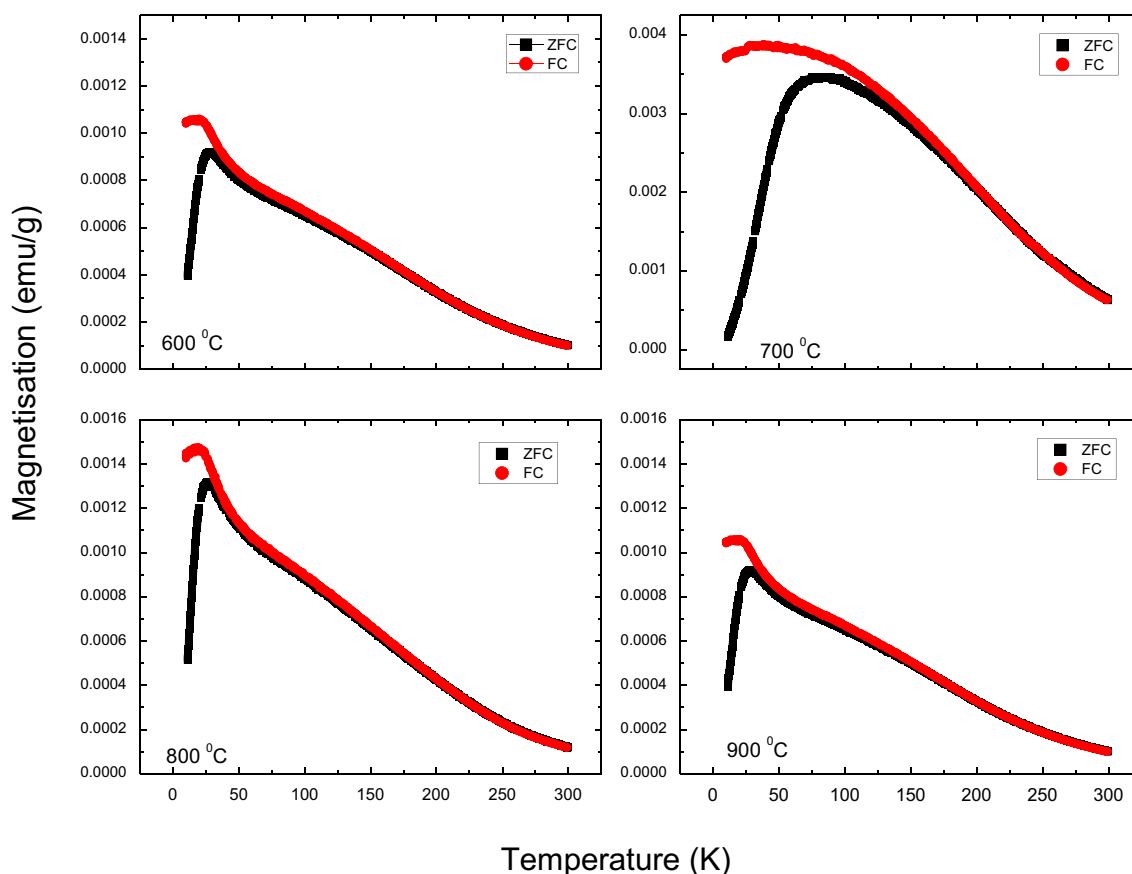
Fig. 7 Temperature-dependent magnetization behavior of the samples annealed at different temperatures

and the blocking temperatures with highest energy barrier related to average blocking temperature. The difference between T_{irr} and T_{max} account for the width of the blocking temperature distribution [27, 28]. ZFC and FC curves significantly diverge below T_{irr} and samples become ferromagnetic state.

4 Conclusion

$Ni_{0.05}Zn_{0.95}Fe_2O_4$ nanoparticles have been synthesized using the sol–gel technique to investigate their structural and magnetic properties as a function of various annealing temperature. Average particle size was obtained between 31.2 and 35.8 nm from XRD analysis. NZFO nanoparticles exhibited the spinel cubic structure without secondary phases but a secondary magnetic phase was obtained by magnetic measurements and this impurity phase effected magnetic characterization of the samples. All samples were not saturated at all temperatures. The reason of this may be explained by the effects of crystal fields and exchange interactions on magnetic properties. There was no correlation between particle size and magnetic properties. Competition

between ferromagnetism and antiferromagnetism interaction exhibited in one system.

References

1. Gorter, E.W.: Saturation magnetization and crystal chemistry of ferrimagnetic oxides. Philips Res. Repts. **9**, 295–320 (1954)
2. Selim, M.S., Turkey, G., Shouman, M.A., El-Shobaky, G.A.: Solid State Ionics. **120**, 173 (1999)
3. Deraz, N.M., Alarii, A.: Structural, morphological and magnetic properties of nano-crystalline zinc substituted cobalt ferrite system. J. Anal. Appl. Pyrolysis **94**, 41–47 (2012)
4. Ozin, G.A.: Characterization of semiconductor heterostructures and nanostructures. Adv. Mater. **4**, 612 (1992)
5. Gleiter, H.: Nanostructured Materials. Adv. Mater. **4**, 474 (1992)
6. Zhou, Z.H., Xue, J.M., Wang, J., Chan, H.S.O., Yu, T., Shen, Z.X.J.: $NiFe_2O_4$ nanoparticles formed in situ in silica matrix by mechanical activation. Appl. Phys. **91**, 6015 (2002)
7. Heiba, Z.K., Mohamed, M.B., Arda, L., Dogan, N.: Cation distribution correlated with magnetic properties of nanocrystalline gadolinium substituted nickel ferrite. J. Magn. Magn. Mater. **391**, 195–202 (2015)

8. Heiba, Z.K., Mohamed, M.B., Wahba, A.M., Arda, L.: Magnetic and structural properties of nanocrystalline cobalt-substituted magnesium–manganese ferrite. J. Supercond. Nov. Magn. **28**, 2517–2524 (2015)

9. Dogan, N., Bingolbali, A., Arda, L., Akcan, D.: Synthesis, structure, and magnetic properties of Ni$_{1-x}$Zn$_x$Fe$_2$O$_4$ Nanoparticles. doi:10.1007/s10948-016-3899-y

10. Shinde, S.S., Jadhav, K.M.: Electrical and dielectric properties of silicon substituted cobalt ferrites. Mater. Lett. **37**, 63–67 (1998)

11. Sawataky, G.A., Van Der Woude, F., Morrish, A.H.: Cation distributions in octahedral and tetrahedral sites of the ferrimagnetic spinel CoFe$_2$O$_4$. J. Appl. Phys. **39**, 1204 (1968)

12. Rondinone, A.J., Samia, A.C.S., Zhang, Z.J.: Characterizing the magnetic anisotropy constant of spinel cobalt ferrite nanoparticles. Appl. Phys. Lett. **76**, 3624–3626 (2000)

13. Pallai, V., Shah, D.O.: Synthesis of high-coercivity cobalt ferrite particles using water-in-oil microemulsions. J. Magn. Magn. Mater. **163**, 243–248 (1996)

14. Skomski, R.: Nanomagnetics. J. Phys. Condens. Matter. **15**, R841–934 (2003)

15. Ramankutty, C.G., Sugunan, S.: Surface properties and catalytic activity of ferrospinels of nickel, cobalt and copper, prepared by soft chemical methods. Appl. Catal. A **218**, 39–51 (2001)

16. Reddy, C.V.G., Manorama, S.V., Rao, V.J.: Semiconducting gas sensor for chlorine based on inverse spinel nickel ferrite. Sens. Actuators B: Chemical **55**, 90–95 (1999)

17. Candlish, I.E., Kear, B.H., Kim, B.K.: Processing and properties of nanostructured WC-Co. Nanostuct. Mater. **1**, 119–124 (1992)

18. Skandan, G., Hahn, H., Roddy, M., Cannon, W.R.: Ultrafine-grained dense monoclinic and tetragonal zirconia. J. Am. Ceram. Soc. **77**, 1706–1710 (1994)

19. Kishimoto, M., Sakurai, Y., Ajima, T.: Magneto-optical properties of Ba-ferrite particulate media. J. Appl. Phys. **76**, 7506–7509 (1994)

20. Li, F., Liu, J.J., Evans, D.G., Duan, X.: Stoichiometric synthesis of pure MFe2O4 (M = Mg, Co, and Ni) spinel ferrites from tailored layered double hydroxide (hydrotalcite-like) precursors. Chem. Mater. **16**, 1597–1602 (2004)

21. Goya, G.F., Rechenberg, H.R.: Ionic disorder and Néel temperature in ZnFe$_2$O$_4$ nanoparticles. J. Magn. Magn. Mater. **196**, 191–192 (1999)

22. Kasapoglu, N., Birsoz, B., Baykal, A., Koseoglu, Y., Toprak, M.S.: Synthesis and magnetic properties of octahedral ferrite NiχCo1−χFe2O4 nanocrystals. Cent. Eur. J. Chem. **5**, 570–580 (2007)

23. Baykal, A., Kasapoglu, N., Koseoglu, Y., Toprak, M.S., Bayrakdar, H.: CTAB-assisted hydrothermal synthesis of NiFe$_2$O$_4$ and its magnetic characterization. J. Alloys Compounds **464**, 514–518 (2008)

24. Lutterotti, L.: Maud 2.33, http://www.ing.unitn.it/~maud/

25. El Sayed, A.M.: Ceram. Int. **28**, 363–367 (2002)

26. Sheikh, A.D., Mathe, V.L.: Anomalous electrical properties of nanocrystalline Ni–Zn ferrite. J. Mater. Sci. **43**, 2018 (2008)

27. Koseoglu, Y., Yildiz, H., Yılgın, R.: Synthesis, characterization and superparamagnetic resonance studies of znfe$_2$o$_4$ nanoparticles. J. Nanosci. Nanotechnol. **12**, 2261–2269 (2012)

28. Nathani, H., Misra, R.D.K.: Surface effects on the magnetic behavior of nanocrystalline nickel ferrites and nickel ferrite-polymer nanocomposites. Mater. Sci. Eng. **113**, 228 (2004)